arXiv:1401.0736v3 [astro-ph.SR] 5 Feb 2014

STEP Team at USTC
http://space.ustc.edu.cn/dreams/

February 6, 2014, 1:16am

When and how does a prominence-like jet gain kinetic energy?

Jiajia Liu,[1] Yuming Wang,[1,*] Rui Liu,[1] Quanhao Zhang,[1] Kai Liu,[1] Chenglong Shen,[1] and S. Wang[1]

[1] *CAS Key Laboratory of Geospace Environment, Department of Geophysics and Planetary Sciences,University of Science & Technology of China, Hefei, Anhui 230026, China*

[*] *Correspondence and requests for materials should be addressed to Yuming Wang (ymwang@ustc.edu.cn)*

Contents

1 Introduction 1

2 Overview 3

3 Axial Motion 3

4 Rotational Motion 5

5 Energy budget 5

6 Conclusions and Discussions 7

Abstract

Jet, a considerable amount of plasma being ejected from chromosphere or lower corona into higher corona, is a common phenomenon. Usually a jet is triggered by a brightening or a flare, which provides the first driving force to push plasma upward. In this process, magnetic reconnection is thought to be the mechanism to convert magnetic energy into thermal, non-thermal and kinetic energies. However, most jets could reach an unusual high altitude and end much later than the end of its associated flare. This fact implies that there is another way to continuously transfer magnetic energy into kinetic energy even after the reconnection. The whole picture described above is well known in the community, but how and how much magnetic energy is released through the way other than the reconnection is still unclear. Here, through studying a prominence-like jet observed by SDO/AIA and STEREO-A/EUVI, we find that the continuous relaxation of the post-reconnection magnetic field structure is an important process for a jet to climb up higher than it could through only reconnection. The kinetic energy of the jet gained through the relaxation is 1.6 times of that gained from the reconnection. The resultant energy flux is hundreds of times larger than the flux required for the local coronal heating, suggesting that such jets are a possible source to keep corona hot. Furthermore, rotational motions appear all the time during the jet. Our analysis suggests that torsional Alfvén waves induced during reconnection could not be the only mechanism to release magnetic energy and drive jets.

1 Introduction

Solar jets are a ubiquitous activity in the solar atmosphere, from active regions, quiet Sun region to polar region. According to their size and observed wavelengths, jets could be classified as surge [e.g., *Newton*, 1934; *Rust*, 1968; *Roy*, 1973; *Xu et al.*, 1984; *Canfield et al.*, 1996; *Jibben and Canfield*, 2004], multi-wavelength (UV, EUV to X-ray) jets [e.g., *Schmieder et al.*, 1988; *Shibata et al.*, 1992; *Cirtain et al.*, 2007; *Culhane et al.*, 2007; *Liu et al.*, 2009; *Shen et al.*, 2011; *Tian et al.*, 2012] and spicules [e.g., *de Pontieu et al.*, 2007a,b; *Shibata et al.*, 2007]. These jets carry lots of mass and energy from low solar atmosphere into corona, and therefore are thought to play an important role in coronal heating and solar wind acceleration [e.g., *Shibata et al.*, 1996, 2007; *Tsiropoula and Tziotziou*, 2004; *de Pontieu et al.*, 2007b].

Previous studies have shown that the length of solar jets range from about one to several hundreds megameter, the speed could be from 10 to thousand kilometers per second, and the lifetime spreads from minutes to hours [e.g., *Shibata et al.*, 1996; *Cirtain et al.*, 2007; *de Pontieu et al.*, 2007a]. Usually, a jet has two components: a hot component and a cool component, which are mainly distributed in the temperature of soft X-ray and 304Å, respectively [e.g., *Moore et al.*, 2013]. Either hot or cool component could be dominant. Therefore some jets are visible in Hα or 304Å passbands, while some jets are visible in EUV or X-ray observations [e.g., *Shen et al.*, 2011; *Srivastava and Murawski*, 2011]. Although different types of jets have different properties, some common phenomena could be found in most cases. The first common phenomenon is flaring, a manifestation of magnetic field reconnection. Except type I spicules [*de Pontieu et al.*, 2007a], stronger or weaker flaring could be always found at the jet root. It is believed to be the initial and major driver of a jet. However, observations showed that the initial speed of a jet usually is too small to make it to a height as observed [e.g., *Roy*, 1973; *Liu et al.*, 2009; *Shen et al.*, 2011], suggesting that some additional force after the flaring must act on the jet plasma.

This fact is closely related with another common phenomenon, apparent rotational/torsional motion of jet plasma during its ascending and/or descending phase [e.g., *Xu et al.*, 1984; *Shibata and Uchida*, 1985; *Canfield et al.*, 1996; *Jibben and Canfield*, 2004; *Shimojo et al.*, 2007; *Liu et al.*, 2009]. A well-accepted picture is that the reconnection between twisted loops and untwisted open field lines causes helicity transferred from loops to open field lines and therefore makes plasma moving upward helically along the path through nonlinear torsional Alfvén waves [e.g., *Pariat et al.*, 2009] or Lorentz force working [*Shibata and Uchida*, 1985]. It is interesting to see which

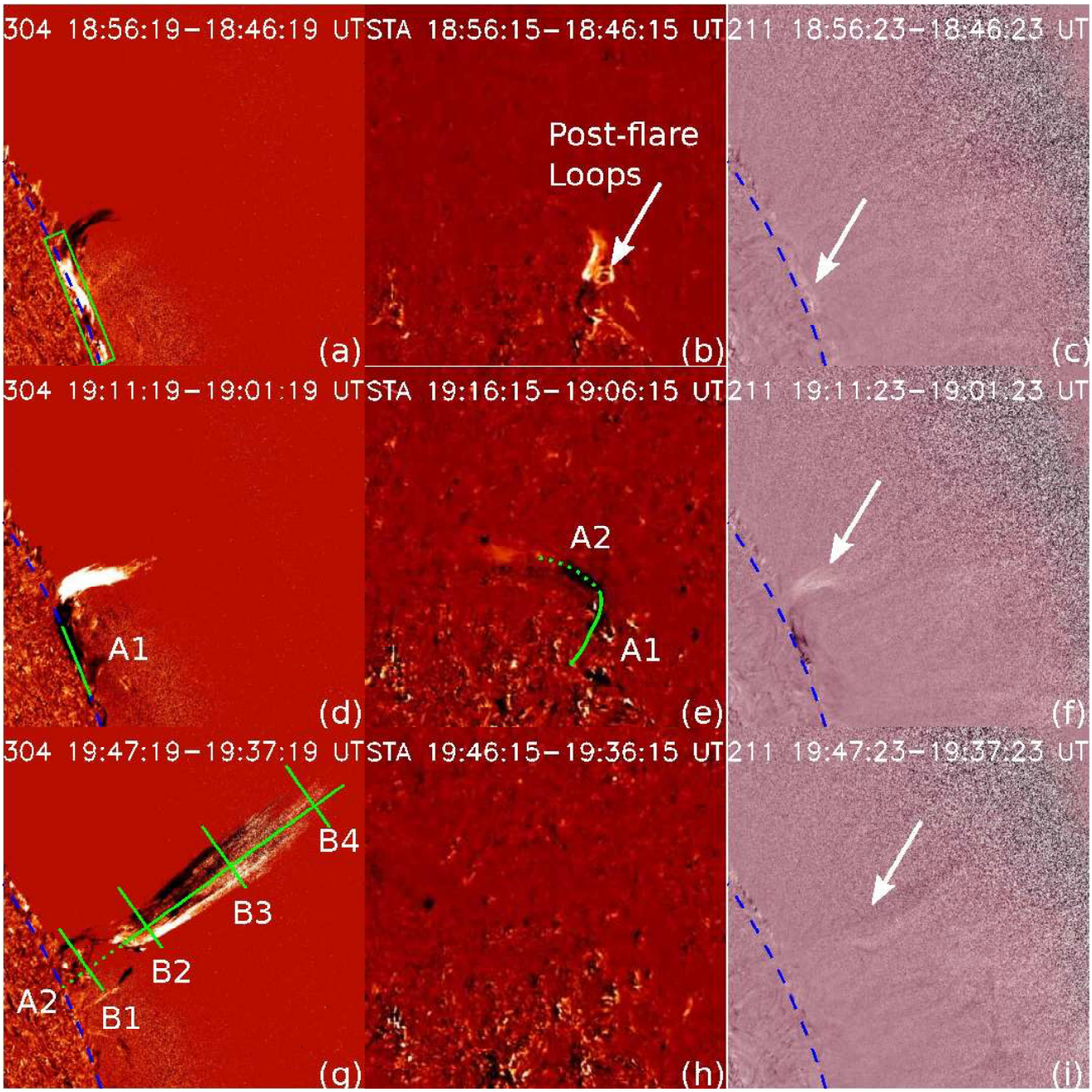

Figure 1: Left column: Difference images taken by SDO/AIA at 304Å passband. The FOV of the images is $430'' \times 430''$. Middle column: Difference images from STEREO-A/EUVI at the same passband. The FOV is $450'' \times 450''$. Since STEREO-A was 120° apart away from SDO on 2012 July 8, the SDO limb event right happened ondisk in the view of STEREO-A. Right column: Difference images taken by SDO/AIA at 211Å passband with the same FOV of the images in the left column. The white arrow in the middle column denotes the post-flare loops and those in the right column mark the hot-component of the jet.

one is more appropriate, or if there is alternative explanation.

One may find that the additional force pushing a jet unusually high is probably just the one driving the apparent rotational motion. In many cases, the jet keeps rising after reconnection. It implies that, during a jet, the magnetic free energy is released through two different ways. One is reconnection, and the other is post-reconnection relaxation of magnetic field structure. Related to the issue raised for the rotational motion, an interesting question is how and how significantly the latter contributes to the jet kinetic energy, or in other words, when and how a jet gains its kinetic energy.

Here, we will try to address this issue by investigating a prominence-like jet that was observed by SDO/AIA [*Lemen et al.*, 2012] and STEREO/SECCHI EUVI [*Howard et al.*, 2008] simultaneously. Thanks to the high-resolution, high-cadence, multi-wavelength and multi-point observations from SDO and STEREO, we are for the first time able to accurately assess its energy budget in observations.

2 Overview

The event located off the north-west limb of the Sun, a bit north to the active region (AR) 11513. Two successive jets can be found at the same place from 18:00 to 21:00 UT on 2012 July 8 in various EUV passbands (see multi-wavelength movie M1). They were the most visible in 304Å, and also showed weak signatures in the hotter channel 211Å (as seen in Fig.1). But the jets were hard to be seen in emission lines with temperature higher than 211Å suggesting that they are cool-component-dominant jets with temperature generally below 2 MK. An online movie M2 generated from AIA 304Å passband shows the detailed ejection process of the two jets. The first jet was a minor one with a life time of about one hour. It began to ascend at about 18:00 UT, reached its maximum height of about 90 Mm 35 minutes later, and then fell back to the solar surface at about 18:56 UT. The second jet is much more significant, which took place right after the first one and lasted for about 2 hours. In this study we will focus on the second jet.

The second jet was triggered by a micro-flare, which caused obvious enhancements of the EUV emissions at various wavelengths as shown in Figure 2 with the peak at about 19:01 UT (indicated by the black dashed line). The core of the micro-flare manifesting as a brightening point first appeared around 18:48 UT at the latitude of about 22°, and then moved on the solar surface to the latitude of about 25°, which probably suggests that the reconnection point was moving. Meanwhile, several brightening small loops appeared beside the brightening point. Accordingly some prominence-like materials traveled along a tunnel lying on the solar surface between the latitude of 22° and 25° at the beginning (see Fig. 1a and 1b).

These materials formed the jet, which started to rise straightly at about 19:05 UT, slightly away from the local radial direction. According to Figure 2 and the online movie M2, the micro-flare faded away around 19:11 UT, suggesting that the reconnection probably lasted for about 23 minutes. At that time the jet was confined within a tunnel with a width of about 15 Mm (Fig. 1d). The rising of the jet could

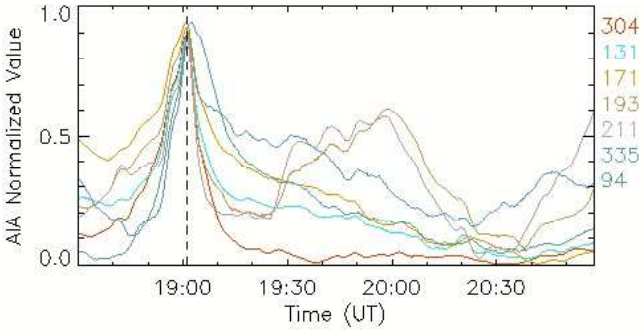

Figure 2: Normalized light curve derived from the integral emission from the brightening region (indicated by the green box in Fig. 1a).

be found in the STEREO-A/EUVI images (Fig. 1e), but the signature is weak due to the relatively low resolution and low cadence of STEREO data.

The jet kept rising after 19:11 UT. It quickly expanded to about 35 Mm wide in a short distance, and gradually grew to about 50 Mm wide when it reached its maximum height of about 292 Mm at about 19:47 UT (Fig. 1g). After then, the jet began to fall back. During the whole ejection process, we can find continuous rotational motion around the jet axis. From the AIA 304Å movie, one can clearly distinguish many pieces of prominence-like materials rotating like a rigid object. In lots of previous studies, the rotational motion appeared only in the ascending phase. Thus torsional Alfvén waves could be a driver of it. However, in this case, the jet plasma kept rotated during its descending phase, and the rotational period did not change significantly as will be seen in Sec.4. This is hard to be explained only by a upward-propagating wave train. This fact spurs us to figure out the real physics behind it. Is the rotational motion the manifestation of real motion of plasma along a twisted magnetic field lines, or a rigid rotation of a bundle of untwisted magnetic field lines? To solve this puzzle, we analyze the axial motion and rotational motion, respectively, in the next two sections.

3 Axial Motion

To study the axial motion of the jet, a slice is placed along the jet tunnel. The slice has two segments; one (labeled as A1 in Fig.1d) lies on the surface and the other (A2, Fig.1g) stands upward straightly. The segment A1 was visible for both SDO and STEREO-A (solid green line in Fig.1e), the projection effect could be easily removed. For segment A2, it is visible for SDO but not all for STEREO-A; only the lower part of A2 can be recognized in STEREO-A/EUVI images (as indicated by the dotted green line in Fig.1e). Thus, we assume that segment A2 is straight and use its lower part to correct the projection effect of A2. It is derived that the segment is about 30° away from the plane-of-sky in the view of SDO. A space-time plot generated from the slice is shown in Figure 3, in which the projection effect has been corrected.

An obvious acceleration could be seen in the plot when the jet moved on the surface. A quadratic fitting to the tracks in the low part of Figure 3 suggests that the acceleration is about 300 m s^{-2}. The jet moved with an aver-

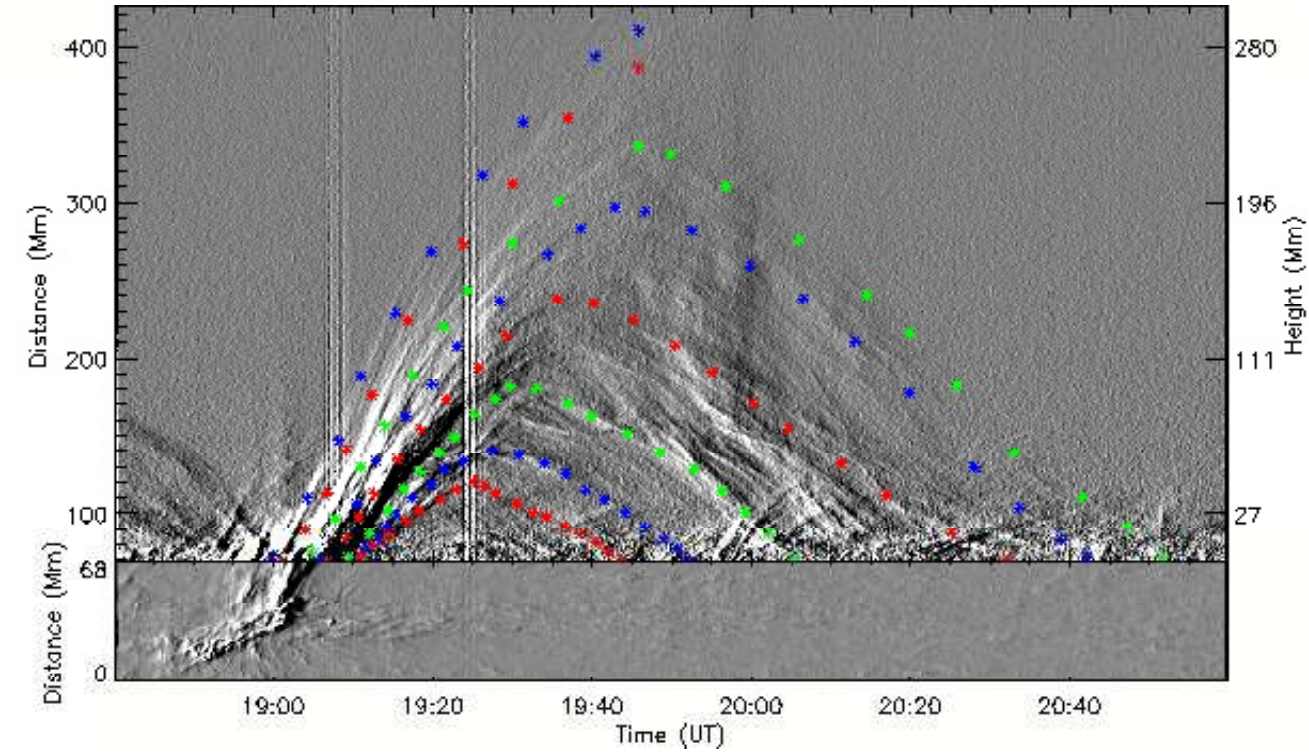

Figure 3: Lower part: De-projected running-difference space-time plot generated from slice A1 (see Fig.1d). Upper part: De-projected running-difference space-time plot generated from slice A2 (see Fig. 1g). The left vertical axis gives the distance from the start point along the slice, and the corresponding height from solar surface is marked on the right vertical axis.

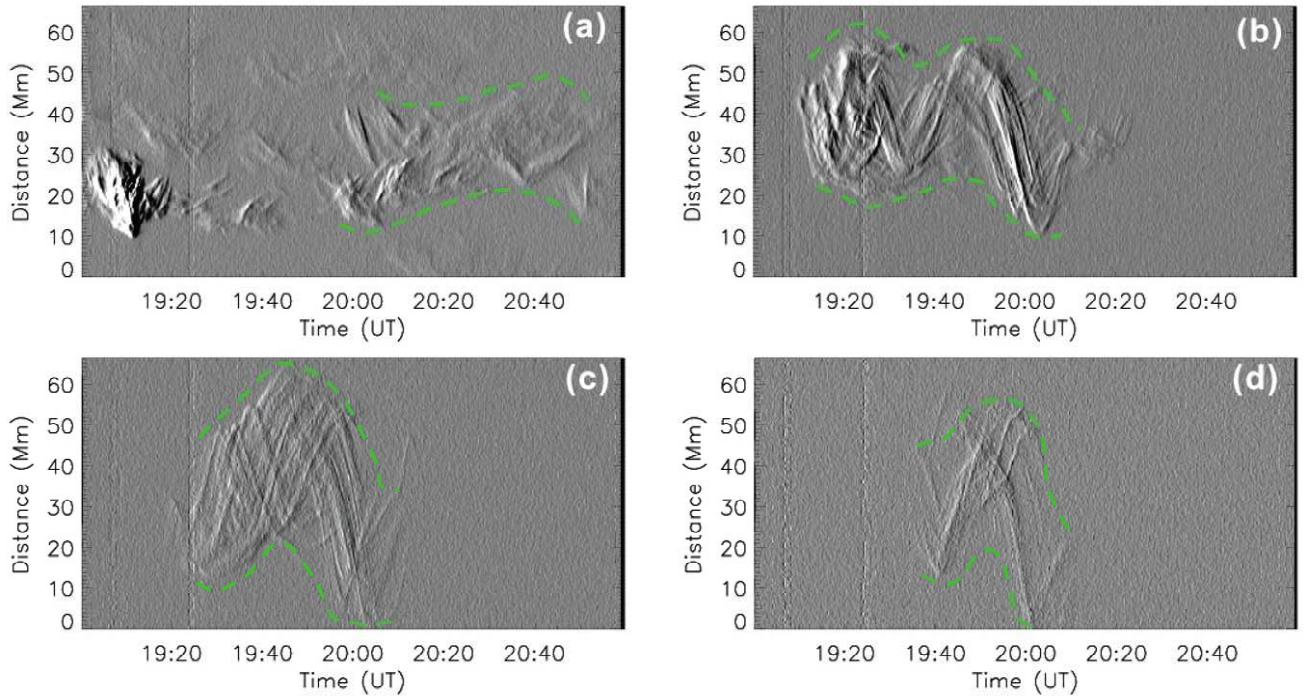

Figure 4: Running-difference space-time plot generated from slice B1, B2, B3 and B4, as marked in Figure 1g. These four slices are all perpendicular to the jet's axis. Dashed lines indicate the boundary of the wriggling jet tunnel.

age velocity of about 95 km s^{-1} and then turned upward with a speed of about 160 km s^{-1} overall. When the jet moved upward, we may distinguish many small sub-jets in it, which are shown as bright-dark alternating stripes in the upper part of Figure 3. These sub-jets were expelled successively. They experienced acceleration at the beginning, and then turned to deceleration. We tracked eight sub-jets as indicated by color-coded asterisks in Figure 3. The initial speeds of these sub-jets ranged from about 57 to 170 km s^{-1}, and through an acceleration, they reached maximum speeds in a range of about 79 to 238 km s^{-1} around 19:11 UT, when the brightening faded away. The earlier sub-jet has a larger acceleration and larger speed. These results are consistent with the fact that the micro-flare decayed with time.

After reaching the maximum upward speed, these sub-jets began to decelerate. Overall, the sub-jets were decelerated during the whole ascending phase, and the deceleration ranged from about -21 to -67 m s^{-2}. These values are smaller than the local gravity, even if the uncertainty (see the note in Table 1) is taken into account. It means that continuous upward force exists after the reconnection. These sub-jets finally reached up to a height from about 42 to 292 Mm (or 120 to 410 Mm in distance along the jet tunnel). Consistent with the speeds obtained before, the earlier sub-jets experienced a longer ascending phase and reached a higher height, which is clearly shown in Figure 3.

The descending speeds of these sub-jets were about -44 to -70 km s^{-1} with an average downward acceleration from -3 to -32 m s^{-2}, which were all smaller than those during the ascending phase. A direct consequence is that the duration of the descending phase is obviously longer than that of the ascending phase. Table 1 lists the kinematic parameters for the eight selected sub-jets.

4 Rotational Motion

In order to analyze the rotational motion of the jet, we place four slices perpendicular to the jet tunnel at the height of 30, 90, 180 and 270 Mm, respectively (marked by B1 to B4 in Fig. 1g). Figure 4 shows the space-time plots generated from the four slices, in which the end of a slice at the higher latitude is referred as zero and stripes with positive slopes indicate motion of material from higher latitude toward lower latitude.

From these plots, we can see many sine-like tracks, suggesting rotational motion in the jet tunnel. Such sine-like tracks appeared during both ascending and descending phases. In particular, these rotating materials seemingly concentrated near the surface of the jet tunnel. According to these tracks, we find that the jet tunnel was wriggling slightly, as indicated by the dashed lines. It is estimated that the width of the jet tunnel at the four heights is about 12, 30, 40 and 45 Mm, respectively.

Assuming that the jet tunnel is a cylinder with a varying radius, the real rotational speed could be derived by fitting these curves with a sine function. Table 2 gives the derived parameters for the rotational motion. It is found that their period is around 1270 s, and there is no significant difference in the period at different heights. The real rotational speed at the four different heights is therefore about 32, 74, 97 and 106 km s^{-1}, respectively. Although these results suffer from a large error, they suggest that the jet material rotated faster and faster as it ascended and then slowed down when it fell back.

As mentioned before, for such an apparent rotational motion, there could be two different interpretations. One is that prominence-like materials move along twisted or helical magnetic field lines, and the other is that a bundle of straight magnetic field lines rotate as a rigid body in which prominence-like materials move up and down. If the first interpretation is the case, we expect that the turns the materials rotated around the jet tunnel within a given distance should be the same for different sub-jets. For sub-jet 1 (see Table 1), the turns per unit length is $n = \frac{1}{T_c v_{avg}} \approx \frac{1}{1270(\mathrm{s}) \times 126(\mathrm{km\ s^{-1}})} = 0.006$ $\mathrm{Mm^{-1}}$. Using this number to constrain sub-jet 7 or 8, we may derive that the expected period of them should be about 2381 or 2976 s, which is much larger than the observed period given in Table 2 even if the uncertainty is taken into account, and cannot be found in the space-time plots.

Thus, the second interpretation is more appropriate. In this scenario, the jet tunnel above the limb consists of straight/untwisted open magnetic field lines. They rotated due to the reconnection at the jet root, which connected the untwisted open magnetic field lines to a bunch of highly twisted magnetic field loops and caused the helicity transported from the twisted fields into untwisted fields. The brightening and small loops shown in the first and second panels of Figure 1 are the signatures. The transport process therefore manifested a rotational motion.

5 Energy budget

During the jet process, some prominence-like materials reached as high as 290 Mm or so, suggesting a significant release of magnetic energy. The release process of the magnetic energy obviously has two stages. The first stage is from 18:48 to 19:11 UT. During the stage, a micro-flare took place and then faded away, and meanwhile, the jet traveled on the solar surface and then climbed up to as high as 100 Mm. The second stage is from 19:11 UT to the end of the event. During the stage, the jet continuously ascended until about 19:47 UT and then fell back. The acceleration is significantly smaller than the solar gravity.

For most of such events, the magnetic energy was released through two ways. One is the magnetic reconnection, during which the free magnetic energy is directly converted to produce both thermal and non-thermal emissions and kinetic energy of plasma jets. The resultant magnetic structure through the reconnection may not be at a stable state. It will further relax its configuration to lower energy level. This becomes the other way to release the free energy. For the first stage, both the ways may take effects, and for the second stage, the second way is the only one. It is not new for us that the magnetic energy could be released in such ways, but it is really unclear whether only one of them or both are important for the ejecta. Flare is much easier to catch people's eyes and usually thought to be the major approach to convert magnetic energy into plasma kinetic energy. How much magnetic energy will be further released after a flare? This question is now be addressed below.

Here we compare two instants. One is at 19:11 UT when the micro-flare ended and the jet roughly reached a maxi-

Table 1: Kinematic parameters of eight sub-jets in the axial direction.

	Ascending Phase					Desceding Phase			
Sub-jet	v_{ini}	v_{max}	v_{avg}	a_{avg}	T_a	v_{avg}	a_{avg}	T_d	H_{max}
1	170±10	238±16	126±2	-56±5	2754	–	–	–	292
2	144±14	193±21	124±2	-49±5	2693	–	–	–	272
3	150±12	178±19	110±2	-56±6	2468	-70±1	-6±2	3943	229
4	140±10	174±18	102±2	-48±7	2222	-68±1	-17±3	3564	196
5	125±19	135±33	100±3	-46±12	1730	-53±1	-3±3	3340	145
6	104±16	122±30	90±4	-35±23	1229	-52±2	-28±8	2130	98
7	75±24	126±53	70±5	-67±31	1075	-49±3	-32±15	1495	61
8	57±27	79±50	56±5	-21±40	957	-44±4	-10±27	1106	42

v_{ini}, v_{max} and v_{avg} are the initial, maximum and average speed, respectively, in units of km s^{-1}. a_{avg} is the average acceleration in units of m s^{-2}. T_a and T_d are the duration in units of second. H_{max} is the maximum height a sub-jet reached, which is units of Mm. The uncertainty in the velocity and acceleration is estimated through the fitting procedure by assuming a 10-pixel error in measuring height (corresponding to a 5-Mm error in distance). Positive values correspond to the upward direction.

Table 2: Kinematic parameters of the rotational motion of the jet.

	H	D	T_c	v_ϕ
B1	30	12	1180±120	32±3
B2	90	30	1270±230	74±13
B3	180	40	1290±330	97±25
B4	270	45	1330±250	106±20

H is the height of the four slices in units of Mm, D is the width (assuming being diameter) of the jet tunnel in units of Mm, T_c is the period of the rotational motion in units of seconds, and v_ϕ is the rotational speed in units of km s^{-1}.

Table 3: Energies of the jet at two instants.

Time	E_g	E_l	E_a	E_t
19:11 UT	0.88	$1.15^{+0.44}_{-0.35}$	$0.11^{+0.03}_{-0.04}$	$2.14^{+0.47}_{-0.39}$
19:47 UT	2.83	$0.08^{+0.08}_{-0.04}$	$0.37^{+0.18}_{-0.14}$	$3.28^{+0.26}_{-0.18}$

Energies are in units of 10^{10} J kg^{-1}.

mum ascending speed (Fig.1d), and the other is at 19:47 UT when the jet reached the maximum height (Fig. 1g). Figure 5 shows the emission intensity, I, as a function of height at the two instants. The emission intensity is calculated based on images in EUV 304Å passband, and it is an integrated value over the cross-section of the jet cylinder at any given height. Here the background emission is removed by subtracting the average value of the pixels surrounding the jet.

The average value I_0 of the intensity of the whole jet is about 216 and 168, respectively, in units of digital number (DN) at the two instants (as indicated by the two horizontal dashed lines in Fig. 5). For prominences observed in 304Å emission line, which is optically thick, it could be accepted that $\rho \propto I$, where ρ is the density. Thus, the product of the average intensity and the height could be a proxy of the mass of the jet material. The difference of the average intensity between the two instants suggests that the mass is not the same, but the difference is relatively small. It may be caused by the errors in measurements or the shielding effect in the optically thick medium.

In order to make the two instants comparative, we investigate the energy per unit mass. According to the distribution of the intensity shown in Figure 5, the gravitational potential energy per unit mass gained by the jet can be calculated by $E_g = GM_\odot \frac{\int_0^H I\left(\frac{1}{R_\odot}-\frac{1}{h+R_\odot}\right)dh}{\int_0^H I dh}$. The kinetic energy per unit mass of the jet consists of two components. One is the linear kinetic energy and the other is the angular kinetic energy, which are given by $E_l = \frac{\int_0^H Iv^2 dh}{2\int_0^H I dh}$ and $E_a = \frac{\int_0^H Iv_\phi^2 dh}{2\int_0^H I dh}$. The linear velocity could be read from Figure 3 and the angular velocity from Table 2. These velocities have been marked as symbols in Figure 5. The velocity between the symbols is obtained by using linear extrapolation, and the velocity outside the symbols just chooses the value of the nearest symbol (as indicated by the dashed lines connecting the symbols).

Table 3 lists the energies per unit mass. First of all, the total energy at 19:47 UT is larger than that at 19:11 UT. Their difference ΔE is about 1.14×10^{10} J kg^{-1}, which is about 3 times of the uncertainties of total energy at each instant, suggesting a significant difference. The micro-flare ended at 19:11 UT, which means that there was a continuous conversion from magnetic energy to potential and kinetic energies after the reconnection. The observed rotational motion suggests that an untwisting process at the root of the jet is responsible for the energy conversion, through which the post-reconnection magnetic field structure relaxes to a lower energy state. The amount of the released magnetic energy could be alternatively estimated from the measurements of the accelerations of sub-jets. Since their acceleration (see a_{avg} listed in Table 1) is much smaller than the gravity, there must be additional force $f = m(a_{avg} - g)$ acting on the jet, where m is the mass and $g = -274$ m s^{-2} is the gravity. The work per unit mass done by the force is $W = fH/m = (a_{avg} - g)H$. According to the values of a_{avg} and H given in Table 1, it is easily inferred that W is on the order of 10^{10} J kg^{-1}, which is consistent with ΔE derived above.

Usually reconnection produces straight plasma beams, like a jet. Thus it is reasonable to assume that the angular ki-

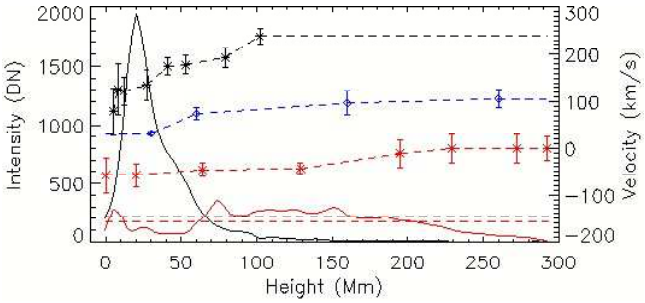

Figure 5: Solid lines show the integrated intensity of EUV 304Å emission over the cross-section of the jet as a function of height, in which the background emission is subtracted. The black line is calculated at 19:11 UT and the red line at 19:47 UT. The mean intensity at the two instants is indicated by two horizontal dashed lines, which are very close to each other. Asterisks connected with dashed lines indicate the axial velocities of the eight sub-jets, and the diamonds connected with dashed lines are the rotational velocities at the four heights.

netic energy E_a should mostly come from the untwisting process. We may infer that, for the kinetic energy (including the potential energy) of the jet, the contribution from the reconnection, i.e., the micro-flare, is $E_r = E_{t0} - E_{a0} = 2.03 \times 10^{10}$ J kg^{-1}, and the contribution from the untwisting process in the ascending phase is $E_{ua} = E_{t1} - E_{t0} + E_{a0} = 1.25 \times 10^{10}$ J kg^{-1}, where the subscript 0 and 1 refers to the instant of 19:11 and 19:47 UT, respectively. Moreover, by considering that (1) the rotational motion continuously existed during the descending phase, (2) the rotational velocity and period are almost as the same as those during the ascending phase and (3) the duration of the descending phase is about 1.57 times of that of the ascending phase (ref. Table 1), we derive that the contribution of the untwisting process during the whole event is roughly $E_u = 2.57 E_{ua} = 3.2 \times 10^{10}$ J kg^{-1}, which is 1.6 times of the kinetic energy that could be injected by the reconnection. Even if considering the kinetic energy produced by a reconnection/flare is only a small fraction (about 10%) of its total released energy [e.g., *Woods et al.*, 2004; *Benz*, 2008; *Reeves et al.*, 2010; *Emslie et al.*, 2012], the contribution of the untwisting process is still significant, which is about 16% of the total released magnetic free energy by a reconnection.

6 Conclusions and Discussions

We presented the observational features of a prominence-like jet event observed by SDO/AIA and STEREO/SECCHI EUVI simultaneously on 2012 July 8. Like most jets observed before, it was triggered by a micro-flare accompanied with several small brightening loops, suggesting a weak reconnection. After obtaining initial momentum, the jet traveled along a tunnel to reach a height of about 292 Mm above the solar surface, and then returned back to the Sun. During the whole process, the acceleration in radial direction is significantly smaller than solar gravity, implying an additional force acting on the jet plasma even after the reconnection. All these observations fit well the classical jet model as proposed in Figure 4 of the paper by *Shibata et al.* [1996].

The magnetic free energy is released through two ways during the jet. One is reconnection and the other is the magnetic field relaxation after the reconnection. By analyzing its motion and energy budget, we find that the magnetic field relaxation after the reconnection makes a significant contribution for the jet to gain kinetic energy, which is about 1.6 times of the contribution made by reconnection, and about 16% of total magnetic free energy that could be released by the reconnection.

Rotational motion is a manifestation of continuously conversion of magnetic energy into kinetic energy through a way rather than the reconnection. In this case, we believe that the twisted loops, which are connected to the untwisted magnetic field lines, drive the rotation. But different from traditional picture, the rotation is probably not mainly caused by torsional Alfvén wave [*Pariat et al.*, 2009]. The reason is that (1) the rotation appeared in both ascending and descending phases, and (2) the additional force preventing the jet plasma falling back is even larger during the descending phase, which caused the descending phase much longer than the ascending phase. These new findings are not expected by the classical jet model. What is the physics behind them is worthy of further study.

A similar picture showing the rotation of a bundle of untwisted (or weak twisted) magnetic field lines could be found in a recent study of solar tornadoes/cyclones [*Wedemeyer-Böhm et al.*, 2012]. In their case, vortex flows at base rather than reconnection drive up flow. Solar cyclones are found to be a ubiquitous phenomenon in the solar atmosphere [e.g., *Brandt et al.*, 1988; *Wedemeyer-Böhm and Rouppe van der Voort*, 2009; *Attie et al.*, 2009; *Zhang and Liu*, 2011; *Wedemeyer-Böhm et al.*, 2012; *Li et al.*, 2012; *Liu et al.*, 2012; *Su et al.*, 2012]. Jets also a ubiquitous phenomenon in the solar atmosphere. Thus we may conjecture that the rotational motion generated during jets, which is usually observed from side-view, and the cyclones that are usually observed from top-view may be probably the same thing, or at least jets are a subset of solar cyclones. For this case, we are unable to make deeper analysis on this issue, because of the low resolution and low cadence of STEREO-A data, although STEREO-A observed the event from another angle of view.

In this case, the conversion rate per unit mass of the magnetic energy to kinetic energy is about $E_u/(T_a+T_d) = 5\times10^6$ J kg^{-1} s^{-1}. By assuming a typical number density of about 10^{10} cm^{-3} of the jet plasma [*Roy*, 1973], the conversion rate per unit volume is about 8×10^{-5} J m^{-3} s^{-1}, and the momentum flux is about 1.7×10^4 J m^{-2} s^{-1} by considering a length scale of about 200 Mm. The radiation of hot corona requires a energy flux of about 3×10^2 J m^{-2} s^{-1} into thermal energy [e.g., *Withbroe and Noyes*, 1977; *Aschwanden*, 2006], which is 2% of the momentum flux of the jet. In other words, the local corona could be heated as long as only a very small fraction of kinetic energy carried by the jet is dissipated. Thus, we believe that jets are able to heat local corona when they get kinetic energy, as suggested in many previous studies for spicules and X-ray jets [e.g., *Tsiropoula and Tziotziou*, 2004; *de Pontieu et al.*, 2007b; *Shibata et al.*, 2007; *Cirtain et al.*, 2007].

Acknowledgments. We acknowledge the use of data from AIA instrument onboard Solar Dynamics Observatory (SDO) and EUVI instrument onboard Solar TErrestrial RElations Observatory (STEREO). This work is supported by grants from the CAS (the Key Research Program KZZD-EW-01-4, 100-talent program, KZCX2-YW-QN511 and startup fund), 973 key project (2011CB811403), NSFC (41131065, 40904046, 40874075, and 41121003), MOEC (20113402110001) and the fundamental research funds for the central universities.

References

Aschwanden, M. J., *Physics of the Solar Corona - An Introduction with Problems and Solutions*, Springer, 2006.

Attie, R., D. E. Innes, and H. E. Potts, Evidence of photospheric vortex flows at supergranular junctions observed by FG/SOT (Hinode), *A&A*, *493*, L13–L16, 2009.

Benz, A. O., Flare Observations, *Living Reviews in Solar Physics*, *5*, 1, 2008.

Brandt, P. N., G. B. Scharmer, S. Ferguson, R. A. Shine, and T. D. Tarbell, Vortex flow in the solar photosphere, *Nature*, *335*, 238–240, 1988.

Canfield, R. C., K. P. Reardon, K. D. Leka, K. Shibata, T. Yokoyama, and M. Shimojo, Hα Surges and X-ray Jets in AR 7260, *ApJ*, *464*, 1016–1029, 1996.

Cirtain, J. W., L. Golub, L. Lundquist, A. van Ballegooijen, A. Savcheva, M. Shimojo, E. DeLuca, S. Tsuneta, T. Sakao, K. Reeves, M. Weber, R. Kano, N. Narukage, and K. Shibasaki, Evidence for Alfvén Waves in Solar X-ray Jets, *Science*, *318*, 1580–1582, 2007.

Culhane, L., L. K. Harra, D. Baker, L. Van Driel-GEsztelyi, J. Sun, G. A. Doschek, D. H. Brooks, L. L. Lundquist, S. Kamio, P. R. Young, and V. H. Hansteen, Hinode EUV Study of Jets in the Sun's South Polar Corona, *PASJ*, *59*, S751–S756, 2007.

de Pontieu, B., S. McIntosh, V. H. Hansteen, M. Carlsson, C. J. Schrijver, T. D. Tarbell, A. M. Title, R. A. Shine, Y. Suematsu, S. Tsuneta, Y. Katsukawa, K. Ichimoto, T. Shimizu, and S. Nagata, A Tale of Two Spicules: The Impact of Spicules on the Magnetic Chromosphere, *PASJ*, *59*, 655, 2007a.

de Pontieu, B., S. W. McIntosh, M. Carlsson, V. H. Hansteen, T. D. Tarbell, C. J. Schrijver, a. M. Title, R. a. Shine, S. Tsuneta, Y. Katsukawa, K. Ichimoto, Y. Suematsu, T. Shimizu, and S. Nagata, Chromospheric Alfvénic Waves Strong Enough to Power the Solar Wind, *Science*, *318*, 1574–1577, 2007b.

Emslie, A. G., B. R. Dennis, A. Y. Shih, P. C. Chamberlin, R. A. Mewaldt, C. S. Moore, G. H. Share, A. Vourlidas, and B. T. Welsch, Global Energetics of Thirty-eight Large Solar Eruptive Events, *ApJ*, *759*, 71, 2012.

Howard, R. A., J. D. Moses, A. Vourlidas, J. S. Newmark, D. G. Socker, S. P. Plunkett, C. M. Korendyke, J. W. Cook, A. Hurley, J. M. Davila, W. T. Thompson, O. C. St Cyr, E. Mentzell, K. Mehalick, J. R. Lemen, J. P. Wuelser, D. W. Duncan, T. D. Tarbell, C. J. Wolfson, A. Moore, R. A. Harrison, N. R. Waltham, J. Lang, C. J. Davis, C. J. Eyles, H. Mapson-Menard, G. M. Simnett, J. P. Halain, J. M. Defise, E. Mazy, P. Rochus, R. Mercier, M. F. Ravet, F. Delmotte, F. Auchere, J. P. Delaboudiniere, V. Bothmer, W. Deutsch, D. Wang, N. Rich, S. Cooper, V. Stephens, G. Maahs, R. Baugh, D. McMullin, and T. Carter, Sun Earth Connection Coronal and Heliospheric Investigation (SECCHI), *Space Sci. Rev.*, *136*, 67, 2008.

Jibben, P., and R. C. Canfield, Twist Propagation in Hα Surges, *ApJ*, *610*(2), 1129–1135, 2004.

Lemen, J. R., A. M. Title, D. J. Akin, P. F. Boerner, C. Chou, J. F. Drake, D. W. Duncan, C. G. Edwards, F. M. Friedlaender, G. F. Heyman, N. E. Hurlburt, N. L. Katz, G. D. Kushner, M. Levay, R. W. Lindgren, D. P. Mathur, E. L. Mcfeaters, S. Mitchell, R. A. Rehse, C. J. Schrijver, L. A. Springer, R. A. Stern, T. D. Tarbell, C. J. Wolfson, C. Yanari, J. A. Bookbinder, P. N. Cheimets, D. Caldwell, E. E. Deluca, R. Gates, L. Golub, S. Park, W. A. Podgorski, R. I. Bush, P. H. Scherrer, M. A. Gummin, P. Smith, G. Auker, P. Jerram, P. Pool, R. Soufli, D. L. Windt, S. Beardsley, M. Clapp, J. Lang, and N. Waltham, The Atmospheric Imaging Assembly (AIA) on the Solar Dynamics Observatory (SDO), *Solar Physics*, *275*, 17–40, 2012.

Li, X., H. Morgan, D. Leonard, and L. Jeska, A Solar Tornado Observed by AIA/SDO: Rotational Flow and Evolution of Magnetic Helicity in a Prominence and Cavity, *ApJ Letters*, *752*, L22, 2012.

Liu, J., Z. Zhou, Y. Wang, R. Liu, B. Wang, C. Liao, C. Shen, H. Zheng, B. Miao, Z. Su, and S. Wang, Slow Magnetoacoustic Waves Observed above a Quiet-Sun Region in a Dark Cavity, *ApJ Letters*, *758*, L26, 2012.

Liu, W., T. E. Berger, A. M. Title, and T. D. Tarbell, An Intriguing Chromospheric Jet Observed By Hinode : Fine Structure Kinematics and Evidence of Unwinding Twists, *ApJ Letters*, *707*(1), L37–L41, 2009.

Moore, R. L., A. C. Sterling, D. A. Falconer, and D. Robe, The Cool Component And The Dichotomy, Lateral Expansion, And Axial Rotation of Solar X-Ray jets, *ApJ*, *769*, 134, 2013.

Newton, H. W., The Distribution of Radial Velocities of Dark Hα Markings near Sunspots, *MNRAS*, *94*, 472, 1934.

Pariat, E., S. K. Antiochos, and C. R. DeVore, A Model for Solar Polar Jets, *ApJ*, *691*(1), 61–74, 2009.

Reeves, K. K., J. A. Linker, Z. Mikić, and T. G. Forbes, Current Sheet Energetics, Flare Emissions, and Energy Partition in a Simulated Solar Eruption, *ApJ*, *721*, 1547–1558, 2010.

Roy, J.-R., The Dynamics of Solar Surges, *Solar Phys.*, *32*, 139, 1973.

Rust, D. M., Chromospheric Explosions and Satellite Sunspots, *LADS*, *35*, 77–84, 1968.

Schmieder, B., G. Simnett, E. Tandberg-Hanssen, and P. Mein, An Example of The Association of X-Ray and UV Emission with Hα Surges, *A&A*, *201*, 327–338, 1988.

Shen, Y., Y. Liu, J. Su, and A. Ibrahim, Kinematics and Fine Structure of an Unwinding Polar Jet Observed By the Solar Dynamic Observatory /Atmospheric Imaging Assembly, *ApJ Letters*, *735*(2), L43, 2011.

Shibata, K., and Y. Uchida, A Magnetodynamic Mechanism for the Formation of Astrophysical Jets. I. Dynamical Effects of the Relaxation of Nonlinear Magnetic Twists, *PASJ*, *37*, 31–46, 1985.

Shibata, K., Y. Ishido, L. W. Action, K. T. Strong, T. Hirayama, Y. Uchida, A. H. McAllister, R. Matsumoto, S. Tsuneta, T. Shimizu, H. Hara, T. Sakurai, K. Ichimoto, Y. Nishino, and Y. Ogawara, Observations of X-Ray Jets with the Yohkoh Soft X-Ray Telescope, *PASJ*, *44*, L173–L179, 1992.

Shibata, K., M. Shimojo, T. Yokoyama, and M. Ohyama, Theory and Observations of X-Ray Jets., in *Astronomical Society of the Pacific Conference Series*, *Astronomical Society of the Pacific Conference Series*, vol. 111, pp. 29–38, 1996.

Shibata, K., T. Nakamura, T. Matsumoto, K. Otsuji, T. J. Okamoto, N. Nishizuka, T. Kawate, H. Watanabe, S. Nagata, S. UeNo, R. Kitai, S. Nozawa, S. Tsuneta, Y. Suematsu, K. Ichimoto, T. Shimizu, Y. Katsukawa, T. D. Tarbell, T. E. Berger, B. W. Lites, R. A. Shine, and A. M. Title, Chromospheric Anemone Jets as Evidence of Ubiquitous Reconnection, *Science*, *318*, 1591–1594, 2007.

Shimojo, M., N. Narukage, R. Kano, T. Sakao, S. Tsuneta, K. Shibasaki, J. W. CIrtain, L. L. LUndquist, K. K. REeves, and A. SAvcheva, Fine Structures of Solar X-Ray Jets Observed with the X-Ray Telescope aboard Hinode, *PASJ*, *59*, S745–S750, 2007.

Srivastava, A. K., and K. Murawski, Observations of A Pulse-driven Cool Polar Jet by SDO/AIA, *A&A*, *534*, A62, 2011.

Su, Y., T. Wang, A. Veronig, M. Temmer, and W. Gan, Solar Magnetized "Tornadoes": Relation To Filaments, *ApJ Letters*, *756*(2), L41, 2012.

Tian, H., S. W. McIntosh, L. Xia, J. He, and X. Wang, What can We Learn about Solar Coronal Mass Ejections, Coronal Dimmings, and Extreme-ultraviolet Jets through Spectroscopic Observations?, *ApJ*, *748*, 106, 2012.

Tsiropoula, G., and K. Tziotziou, The role of chromospheric mottles in the mass balance and heating of the solar atmosphere, *A&A*, *424*, 279–288, 2004.

Wedemeyer-Böhm, S., and L. Rouppe van der Voort, Small-scale swirl events in the quiet Sun chromosphere, *A&A*, *507*, L9–L12, 2009.

Wedemeyer-Böhm, S., E. Scullion, O. Steiner, L. R. van der Voort, J. de la Cruz Rodriguez, V. Fedun, and R. Erdélyi, Magnetic Tornadoes as Energy Channels into the Solar Corona., *Nature*, *486*(7404), 505–508, 2012.

Withbroe, G. L., and R. W. Noyes, Mass and Energy Flow in the Solar Chromosphere and Corona, *ARA&A*, *15*, 363–387, 1977.

Woods, T. N., F. G. Eparvier, J. Fontenla, J. Harder, G. Kopp, W. E. McClintock, G. Rottman, B. Smiley, and M. Snow, Solar irradiance variability during the october 2003 solar storm period, *Geophysical Research Letters*, *31*(10), L10,802, 2004.

Xu, A., D. Ping, and S. Yin, The Rotation Mass Motion in Solar Surge, *ACTA Astronomica Sinica*, *25*, 119–126, 1984.

Zhang, J., and Y. Liu, Ubiquitous Rotating Network Magnetic Fields and Extreme-Ultraviolet Cyclones in the Quiet Sun, *ApJ Letters*, *741*, L7–L11, 2011.